



Adaptive Cardinal Heading Aided for Low Cost Foot-Mounted Inertial Pedestrian Navigation

Khairi Abdulrahim^{1*}, Terry Moore²

¹Faculty of Engineering & Built Environment
Universiti Sains Islam Malaysia, Nilai, 71800, MALAYSIA

²Nottingham Geospatial Institute,
University of Nottingham, NG7 2TU, UNITED KINGDOM

*Corresponding Author

DOI: <https://doi.org/10.30880/ijie.2021.13.04.003>

Received 17 June 2020; Accepted 21 January 2021; Available online 30 April 2021

Abstract: The use of a low-cost MEMS-based Inertial Measurement Unit (IMU) provides a cost-effective approach for navigation purposes. Foot-mounted IMU is a popular option for indoor inertial pedestrian navigation, as a small and light MEMS-based inertial sensor can be tied to a pedestrian's foot or shoe. Without relying on GNSS or other external sensors to enhance navigation, the foot-mounted pedestrian navigation system can autonomously navigate, relying solely on the IMU. This is typically performed with the standard strapdown navigation algorithm in a Kalman filter, where Zero Velocity Updates (ZVU) are used together to restrict the error growth of the low-cost inertial sensors. ZVU is applied every time the user takes a step since there exists a zero velocity condition during stance phase. While velocity and correlated attitude errors can be estimated correctly using ZVUs, heading error is not because it is unobservable. In this paper, we extend our previous work to correct the heading error by aiding it using Multiple Polygon Areas (MPA) with adaptive weighting factor. We termed the approach as Adaptive Cardinal Heading Aided Inertial Navigation (A-CHAIN). We formulated an adaptive weighting factor applied to measurement noise to enhance measurement confidence. We then incorporated MPA heading into the algorithm, whereas multiple buildings with the same orientation are grouped together and assigned a specific heading information as a priori. Results shown that against the original CHAIN, the proposed Adaptive-CHAIN improved the position accuracy by more than five-fold.

Keywords: Foot-mounted, pedestrian navigation, MEMS, zero velocity update

1. Introduction

Pedestrian navigation particularly in non-GNSS (Global Navigation Satellite System) environments is extremely challenging due to the unavailability of useful GNSS signal for positioning. Although High Sensitivity (HS) receiver can be used to detect weak GNSS signal for positioning, often the signal is not reliable enough to produce good position solutions due to errors such as multipath [1]. Therefore, whenever GNSS navigation is not possible, Inertial Navigation System (INS) is commonly used to bridge outages. It has the advantage that no infrastructure is needed and, once initialized, the system is completely self-contained. The system, which normally consists of three accelerometers and three gyroscopes, is small, low power, and inexpensive due to the advances in Micro-electromechanical Sensors (MEMS) technology. However due to the low performance of low-cost MEMS IMU sensor, it is often integrated with other systems to aid the position solution and as a result, the solution is very much dependent on the accuracy of the external system used. For a low cost self-contained system, a popular approach of attaching the IMU on foot or shoe is often adopted,

shown in Fig.1 below, with particular attention is given to finding a way to reduce the heading drift error, which is the primary error in the system in indoors and dense urban environment where pedestrian is likely to walk along.



Fig. 1 - Inertial sensor attached to a shoe

The approach was chosen mainly because of the successful attempt by many [2]–[6] to restrict some of MEMS IMU errors that grow with time. By strapping the IMU on foot or shoe (written as on foot afterwards for generality), zero velocity event during stance phase can be detected by the IMU. As a result, zero velocity update (ZVU) [7]–[11] can be used to give extra measurement update to the estimation filter such as Kalman filter. Nonzero velocity measurement during this period will be viewed as an error, and using the correlation between velocity error and attitude error, IMU errors can be estimated by Kalman filter.

However, one of the problems that remains; apart from the initialization problem (where initial position, velocity and attitude must be obtained from external measurement), is heading drift during navigation. Heading drift still remains despite using ZVU measurements in the Kalman filter because the IMU yaw error is unobservable [12]–[16]. Magnetometers are often used because they are often packed with accelerometers and gyros in an IMU, but their measurements are unreliable when navigating in dynamic environments such as indoors where significant magnetic disturbances occur. Although it has been demonstrated recently [17]–[20] that navigating in indoor environment is possible using magnetometer, it was also highlighted that there is a requirement to have a pre-surveyed magnetic map for that particular buildings which is not quite practical. In [21], it was also shown that consistent update frequency of the magnetometer measurement plays an important role, which is often not the case in indoors due to disturbances. Unless the magnetic disturbances can be accurately modeled and pre-surveyed magnetic map can be used accurately even with the change in magnetic mappings over time, together with consistent update rate, it is therefore desirable to use other means to control heading drift for low cost inertial navigation system.

Previous work by authors successfully addressed the problem using a simple idea of aiding the navigation system using known building heading known as Cardinal Heading Aided Navigation system [22]–[24]. This paper extends this previous works, by proposing to include a construction of multiple polygon areas with adaptive measurement noise for a case when traversing between environments or building with different orientation. Unlike in the previous work by author whose building heading is derived from map, heading information for specific building is assumed to be known in advance. This is not impractical because usually each building is a permanent building and can have its own heading surveyed once and stored in a database. This is quite convenient from the user's point of view since only one update from this information is required to navigate; hence continuous updates from maps are not required. Furthermore, there is no requirement for detailed room-level maps of the areas where the user will navigate. The assumption that the orientations of the building are usually rectangular in shape are also considered in this paper. Although by no means all buildings are constructed in this way, a good number of buildings are. It is indeed considered as a valid assumption; for example [25] wrote that 83.2 % of high rise buildings in Kuala Lumpur, capital city of Malaysia, consists of building with square and rectangular shape. Similarly, dense urban environments are made up of buildings that are typically in sync with each other. This creates a huge area where most buildings in this area have similar orientation.

The contributions of this paper are i) detail explanation on potential way to generate heading information from a given image, ii) the inclusion of multiple polygon areas to store heading information to allow seamless traversing between environment, and iii) the formulation of weighted measurement noise that adaptively follows the generated heading error measurement.

The paper is organized as follows. Section 2 outlines necessary preliminaries strapdown inertial navigation equation, Kalman filter and observability. Section 3 presents the proposed Adaptive Cardinal Heading Aided for Indoor Navigation (A-CHAIN). Section 4 provides results and discussion from 3 real field trials conducted, and followed by conclusion in Section 5.

2. Preliminaries

2.1 Navigation Equation

Kalman filter, and many of its variations, is an optimal state estimation method and is widely recognized and extensively reported in literature. An error-state Extended Kalman filter (EKF) is used [26]–[28].

$$\delta \mathbf{x} = [\delta \mathbf{r}^n \delta \mathbf{v}^n \delta \boldsymbol{\phi}^n \beta_g \beta_a]^T \quad (1)$$

where $\delta \mathbf{r}^n$ is the vector of latitude, longitude and height errors, $\delta \mathbf{v}^n$ is the vector of navigation frame velocity errors, $\delta \boldsymbol{\phi}^n$ is the vector of navigation frame attitude errors, β_g is the vector of gyro bias and β_a is the vector of accelerometer bias. The filter is used in feedback form where errors calculated from the EKF are used to correct the inertial sensor measurements and navigation parameters. Standard strapdown navigation mechanization equations [29]–[31] are used. Velocity error states and attitude error states are propagated using a ϕ -angle error model [29], [32]–[34]:

$$\delta \dot{\mathbf{r}}^n = -\boldsymbol{\omega}_{en}^n \times \delta \mathbf{r}^n + \delta \mathbf{v}^n \quad (2)$$

$$\delta \dot{\mathbf{v}}^n = \mathbf{C}_b^n \delta \mathbf{f}^b + \mathbf{C}_b^n \mathbf{f}^b \times \delta \boldsymbol{\phi} + \delta \mathbf{g}^n - (\boldsymbol{\omega}_{ie}^n + \boldsymbol{\omega}_{in}^n) \times \delta \mathbf{v}^n - (\delta \boldsymbol{\omega}_{ie}^n + \delta \boldsymbol{\omega}_{in}^n) \times \mathbf{v}^n \quad (3)$$

$$\delta \dot{\boldsymbol{\phi}}^n = -\boldsymbol{\omega}_{in}^n \times \delta \boldsymbol{\phi} + \delta \boldsymbol{\omega}_{in}^n - \mathbf{C}_b^n \delta \boldsymbol{\omega}_{ib}^b \quad (4)$$

where $\delta(\cdot)$ represents the error of specific vectors, $\boldsymbol{\omega}_{en}^n$ is the navigation transport rate, \mathbf{C}_b^n is the rotation matrix that transforms from body frame to navigation frame, $\delta \mathbf{g}^n$ is the gravity error vector, $\boldsymbol{\omega}_{ie}^n$ is the Earth's rotation rate and $\boldsymbol{\omega}_{in}^n$ is the navigation turn rate.

Equation (2), (3) & (4) can be simplified by excluding the Earth's rotation rate, navigation transport rate & turn rate and gravity error when a low-cost IMU is used [35]. This is because the IMU is not capable to measure them, and navigation is performed with a low velocity in a relatively small area. The terms $\delta \mathbf{f}^b$ and $\delta \boldsymbol{\omega}_{ib}^b$ represent the errors in accelerometers and gyros respectively. Theoretically, these errors terms can be refined by modelling all possible IMU error terms such as temperature dependent errors and misalignment errors. However, the observability of all the error states, even if it is theoretically possible, is almost impossible because of operational conditions such as requiring sufficient dynamics and long data collection. Both sensor error terms are therefore considered to only consist bias terms and noise (w_g, w_a):

$$\delta \mathbf{f}^b = \beta_a + w_a \quad (5)$$

$$\delta \boldsymbol{\omega}_{ib}^b = \beta_g + w_g \quad (6)$$

Standard EKF equations are used to predict and update the states [36]. For clarity, the discrete measurement model can be written as:

$$\delta \mathbf{z}_k = \mathbf{H} \delta \mathbf{x}_k + \mathbf{n}_k \quad (7)$$

where $\delta \mathbf{z}_k$ is the error measurements, \mathbf{H} is the measurement matrix, and \mathbf{n}_k is the measurement noise with covariance matrix $\mathbf{R}_k = E[\mathbf{n}_k \mathbf{n}_k^T]$.

The updated error state $\delta \mathbf{x}_{k|k}$ at time k is computed when a measurement at time k is available using:

$$\delta \mathbf{x}_{k|k} = \delta \mathbf{x}_{k|k-1} + \mathbf{K}_k [\mathbf{m}_k - \mathbf{H} \delta \mathbf{x}_{k|k-1}] \quad (8)$$

where \mathbf{K}_k is the Kalman gain, \mathbf{m}_k is the actual error measurement, and $\delta \mathbf{x}_{k|k-1}$ is the predicted error state. The Kalman gain is calculated with the usual formula:

$$\mathbf{K}_k = \mathbf{P}_{k|k-1} \mathbf{H}^T (\mathbf{H} \mathbf{P}_{k|k-1} \mathbf{H}^T + \mathbf{R}_k)^{-1} \quad (9)$$

where $\mathbf{P}_{k|k-1}$ is the estimation error covariance matrix, that is computed at time k based on measurements received at time k-1.

2.2 ZVU and Obervability

ZVU measurements are used to update the filter whenever the pedestrian takes a step. When walking, there are two phases of a step, which are swing phase and stance phase. During stance phase, all velocity vectors are assumed to be zero, which is a true assumption since the foot is not moving, and these pseudo-measurements are used to correct the velocity error state in the filter.

Using simplified model, equation (3) can be rewritten as

$$\begin{bmatrix} \delta v_N \\ \delta v_E \\ \delta v_D \end{bmatrix} = \begin{bmatrix} \mathbf{0} & -f_D & -f_E \\ f_D & \mathbf{0} & -f_N \\ f_E & f_N & \mathbf{0} \end{bmatrix} \begin{bmatrix} \delta\varphi \\ \delta\theta \\ \delta\psi \end{bmatrix} + \mathbf{C}_b^n \delta f^b \quad (10)$$

where $\delta\varphi, \delta\theta, \delta\psi$ are roll, pitch and yaw errors respectively. During stance phase, the horizontal forces in the local level frame are essentially zero and specific force f_D in downward direction is approximately close to the negative gravity constant. The velocity errors in North and East directions are related to errors in roll and pitch via a specific force f_D in downwards direction. The roll and pitch errors are always observable through velocity updates because the force in the Down direction is always large as a result of the gravity force, which acts as an 'inclinometer'. The yaw error however is only observable through the horizontal force terms. To observe yaw error, the horizontal force must not be zero, which is not the case for the low-cost foot mounted pedestrian navigation during stationary condition when ZVU is performed. The yaw error is therefore not observable because there is no horizontal force observed during stance phase.

3. Adaptive Cardinal Heading Aided for Indoor Navigation (A-CHAIN)

Cardinal Heading Aided for Indoor Navigation (CHAIN) algorithm was first introduced in [22]–[24]. It takes the difference between heading measurement generated from the current step and the previous step, with the heading information extracted from building orientation to correct the attitude error states. One of the most significant findings, apart from not needing any extra aiding sensors, was that the heading error measurement does not relate directly to the physical attachment of the IMU, which means the IMU can be mounted in any orientation on the user's foot. This was considered very noteworthy because it does not matter if the pedestrian is walking sideways or even backwards for the algorithm to work. In this work, the algorithm is extended to address when pedestrian moves between different buildings. The 'adaptive-CHAIN (A-CHAIN)' term is coined to show how the algorithm adapts to the situation by properly obtaining the heading measurement using multiple polygon areas and weighting the heading measurement noise accordingly.

3.1 Generation of Building Heading

This section details the procedure to generate the heading information. Heading of a building can be derived automatically using a free map. Street level maps, including world map, topographic map and geological map, are very useful for street-level navigation. It provides useful street level information to users that include features such as buildings outline and roads, and uses either line map (2D representation) or aerial imagery (3D-like representation). An extra piece of information commonly found from this type of map is that the map is orientated such that the North is always pointing straight up, East to the right, West to the left and South is pointing to the bottom of the map. This important map information is therefore used, along with a classical edge detection algorithm to show the concept of deriving building heading from minimal map information.

There are many methods for edge detection, but Canny method is chosen as it is the simplest method and commonly used in digital image processing [37]. It works by looking for the minimum and maximum value in the first derivative of an image pixel values. Points that sit within this threshold will be detected as edge points.

After that, Hough Transform [38] is used to detect straight line features from the building image. This is done primarily because edge detection shows where edges are, but not what they are geometrically such as line or arcs. The idea of Hough Transform is that if certain points satisfy the line equation, then it will be considered as a straight line. The longest detected straight line is then selected for reliability purpose as quite often short straight feature does not present the true building orientation. The start and end point of this line are then stored in terms of pixel values and then the equation below is used:

$$\psi^b = \tan^{-1}(\delta y, \delta x) \quad (11)$$

where ψ^b is a derived building heading, δy is the difference between start and end y-pixel value, δx is the difference between start and end x-pixel value. Fig. 2 shows example of the derived heading. The red line is the longest straight-line feature detected in the image with a computed heading to be 37.88° . After the building heading is acquired, a simple offset of 90° is added to the remaining three headings to make up the four derived building headings of 37.88° , 127.88° , 217.88° and 307.88° .

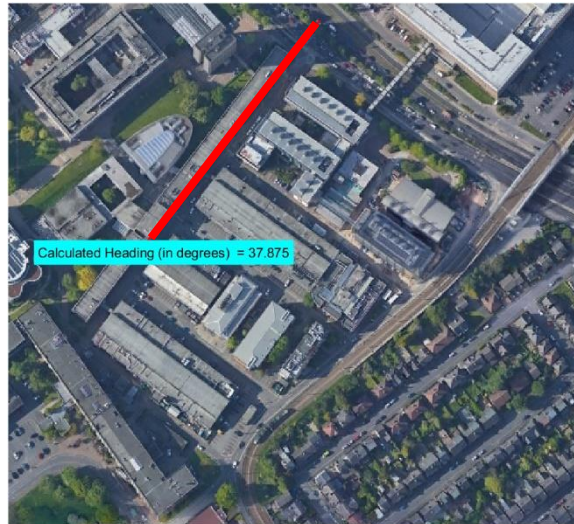


Fig. 2 - Building image with computed heading

3.2 Multiple Polygon Areas

The new multiple headings information is generated using a predefined ‘polygon area’ that was created to contain heading information, and as the user walks, the system is adapted to the new heading information. A simple and well known algorithm, widely known as point in polygon test in computer graphics [39] is adopted where a point is tested to be located inside or outside a certain 2D polygon area (written as ‘polygon’ afterwards). A polygon is generally defined as a set of a finite sequence of straight lines or straight edges that make up a closed path, whilst the points where two edges or lines meet are called polygon’s vertices.

Consider a polygon that contains K vertices (x_n, y_n) where n ranges from 1 to K . Now the problem is how to test whether a point (x_p, y_p) is indeed inside this polygon. Imagine a line is extended horizontally from (x_p, y_p) . The test begins by checking: if the number of times this line intersects the polygon edges is even, then the point is outside the polygon and if the number of intersections is odd, then the point (x_p, y_p) is inside the polygon. Fig. 3 shows the extended line for some sample points A, B and C (denoted by dots). It describes more clearly on how the check is run to determine whether a point lies inside or outside the polygon. For point A and B, the extended lines intersect with the edges for odd times (1 x and 3 x), hence they are located inside the polygon. On the other hand, point C line intersects with the edges for even time (2 x), hence it is considered to be outside the polygon area. To avoid the problem when an edge of the polygon lies on the same line from (x_p, y_p) , the polygon area is constructed such that it is always bigger than the building. By doing this, the position solution from INS will never go beyond polygon boundary; therefore, there will be no occasion where the extended line from the test point overlaps horizontally with the edges.

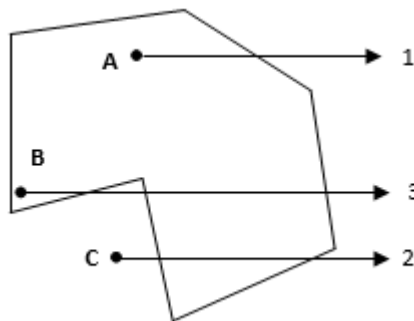


Fig. 3 - The point in polygon test

After the algorithm has been set up, a set of geodetic points are constructed so that it makes up a polygon area of the trial buildings. Multiple Polygon Areas (MPA) are created where each polygon area covers specific trial building and contains heading information for that building. Using a freely available tool in Google Earth, the polygon area is manually constructed for the trial area and it contains four polygon areas that have four different headings.

The algorithm works by testing the test points against the constructed polygon area. The test points are represented by each estimated coordinates (latitude and longitude), calculated from the INS mechanization. As the user walks, the current estimated coordinate will be compared to the polygon area coordinates. If the estimated coordinate lies in any of the polygon areas, then that polygon area is chosen. This selected polygon area, which contains specific building heading information for that area, will then be used as the current building heading for INS, and a similar step as in the previous sections will be performed to update the KF.

Fig. 4 shows four polygon areas constructed for the trial and are marked as areas A, B, C and D. Area A is represented by a cyan line, B by a blue line, C by a green line and D by a white line. It covers a total area of approximately \$2.5 \text{ km}^2\$, with multiple buildings that have a common heading (for example polygon C) are put together into one polygon area.

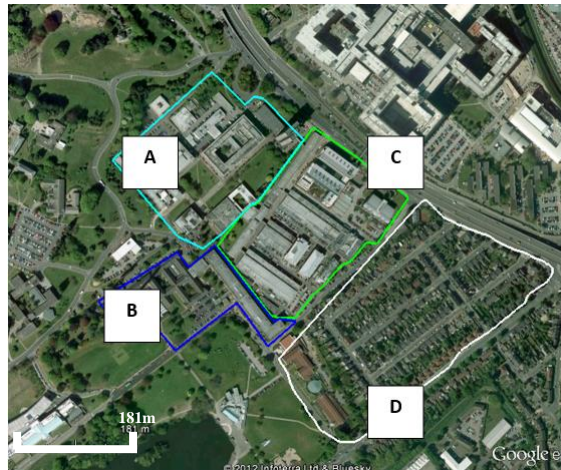


Fig. 4 - Four constructed polygon areas

3.3 Adaptive Weighted Measurement

In our previous work [24], the measurement noise \mathbf{n}_k with covariance $\mathbf{R}_k = (\sigma^2)$ was set experimentally with a constant value. In this work, to eliminate overconfidence in the heading measurement, the covariance is weighted adaptively based on the measured heading error. Depending on which heading information is extracted from the multiple polygon areas, the measurement covariance \mathbf{R}_k is updated with a weighting factor:

$$\mathbf{R}_k = E[\mathbf{n}_k \mathbf{n}_k^T] = \frac{1}{\sqrt{|\psi_s - \psi^b|}} (\sigma^2) \tag{12}$$

where ψ_s is the heading generated from a step, and ψ^b is the building heading from Eq. (11). The covariance is multiplied with the inverse of this difference, whereby it becomes the weighting factor used for every epoch whenever there is a measurement update available to correct the heading. The equation shows that if the heading difference generated is big, which means there is a need to correct this error quickly, then the confidence is increased by reducing the measurement noise covariance. This in turn will increase the Kalman gain accordingly in the filter through Eq. (9). Likewise, if the difference generated is small, then the confidence is decreased by increasing the measurement noise covariance. Note that, the heading measurement in A-CHAIN algorithm is used to update the filter, only when the difference between heading generated from a step and the building heading from the map falls below certain threshold set experimentally in the algorithm to qualify as walking in a straight line [22]. This means, even if the heading difference is big, but if it is above the set threshold, then the adaptive weighted measurement will not be used to update the filter.

4. Results

Three trials representing pedestrian navigation in typical pedestrian environment were performed: 1-Walking indoors in a building, 2-Walking indoors and outdoors within multiple buildings and areas, and 3-Walking outdoors around square pitch. The forward solution estimated from Kalman filter was compared with HSGPS solution and ZVU-only solution, whenever applicable. A Return Position Error (RPE) indicator is used to estimate the accuracy of the trials. The RPE is defined as the error calculated from the difference in start and end position, which means an ideal system would result in RPE value of 0 m. Except for Trial 3, individual position error in every time epoch is not calculated because it is almost impossible to get a ground truth using GNSS measurements due to unavailability of GNSS signals indoors. Even if there is, errors due to multipath and intermittent availability of the signals give erroneous position error. Therefore positions were plotted on Google Earth images for visualization purpose and through this visualization, comparison of position

errors was then made. For all trials, a MicroStrain 3DM-GX3-25 IMU was used which has typical technical specifications of a low cost IMU [40].

Trial 1 involves walking in a typical public building. The walk started and ended at approximately the same position, lasted for about 30 minutes for a total distance of about 2 km. Fig. 5 shows the trajectory solution of the low-cost foot-mounted pedestrian navigation without MPA and is depicted by a green line. The blue line represents the solution with only ZVU to update the filter, while the red dots represent the High Sensitivity GPS (HS-GPS) solution.

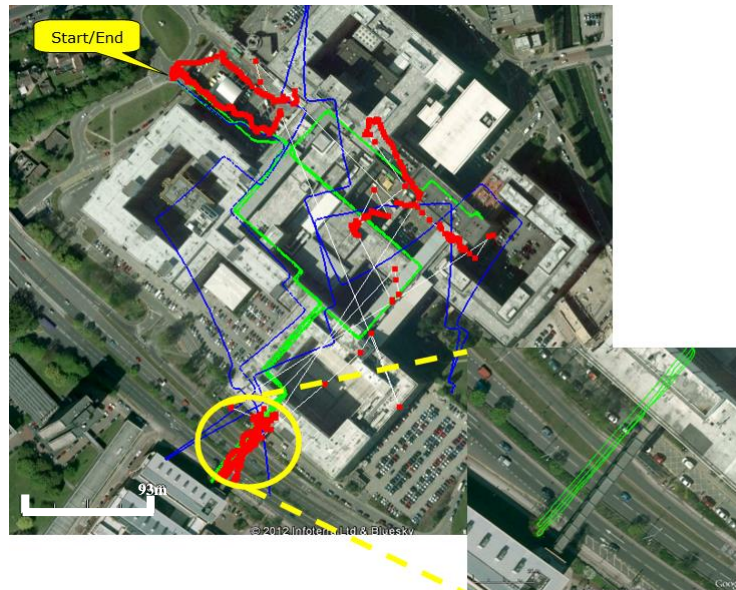


Fig. 5 - The position solutions of HSGPS (red), foot-mounted IMU + ZVU (blue), foot-mounted IMU + ZVU + CHAIN (green)

For ZVU-only approach (blue line), the RPE was 299.71 m, which is about 15 % from the total distance travelled. Conversely, the RPE for the (green line) was found to be 4.63 m, which is about only 0.23 % from the total distance travelled. This contributes more than fifty-fold in position improvement. Although there are some parts where the GPS signal can be detected, the reliability of HSGPS solution (red dots) is questionable because of jumps in the solution. Since this trial did not use the MPA approach, the solution at the bridge area (zoomed figure) gives sub-optimal result because of the different orientation of the bridge from the main building. Therefore, a second trial is conducted next to highlight the adaptive-CHAIN approach.

Trial 2 involves walking in multiple polygon areas, identified as shown in Fig. 4. The trial lasted for about 43 minutes with a distance of about 3.3 km. The area covered is estimated to be about 2.5 km². As before, a pedestrian equipped with only the low-cost foot mounted IMU, started the walk in area C. The pedestrian then moved to area A, after which he walked towards area B, followed by area D and then came back to the start position in area C. Fig. 6 (left) shows the trajectory solution of the low-cost foot-mounted IMU aided by only ZVU and is depicted by a red line, while Fig. 6 (right) shows the trajectory with the system aided by ZVU + adaptive-CHAIN depicted by a green line. Remarkably, the low-cost foot-mounted IMU trajectory follows the trial path (the trial path was obtained from the knowledge of the trajectory during the trial) right until the end of the trial, as opposed to normal IMU-ZVU (the accuracy throughout the trial is not known as only occasional GNSS solutions were available). For this trial, the RPE for the proposed system shown in Fig. 6 (right) was 4.28 m, about 0.13 % from the total distance travelled.

Note that the polygon area D does not consist of only multiple buildings, but an area with about the same orientation with a distinct feature such as straight roads and fences. This highlights the strength of adaptive-CHAIN, where distinct features within an area can be easily extracted from aerial imagery to provide heading information that can be grouped together into an MPA, to which a user is likely to travel if they are in the vicinity of these particular features. For example, a user walking alongside the fence is likely to follow the heading defined by the fence. Similarly, a user walking alongside the building is likely to follow the heading defined by the building.

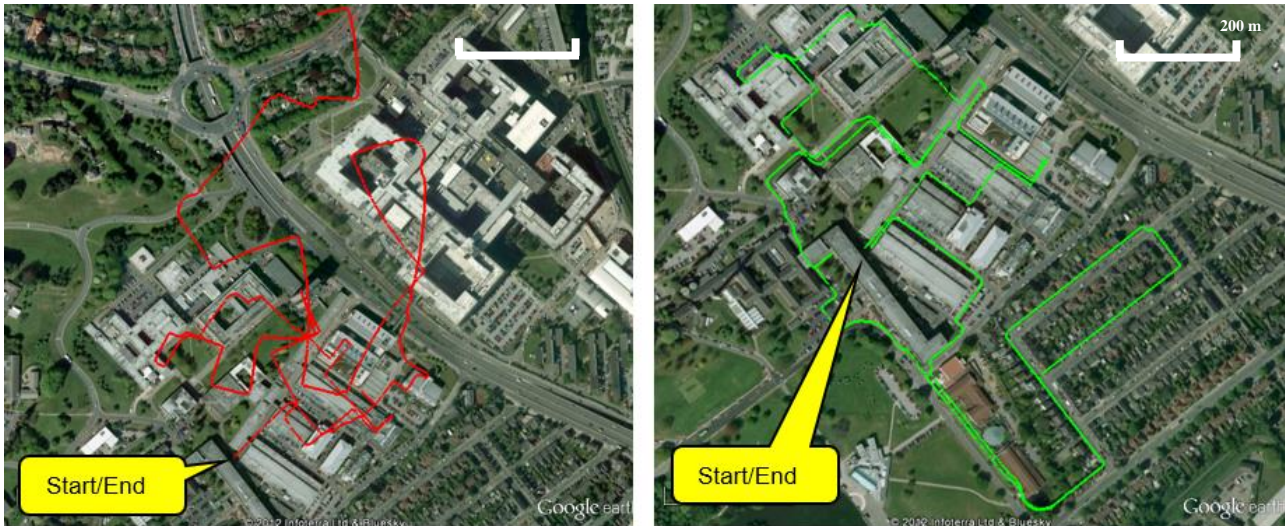


Fig. 6 - Low-cost foot-mounted IMU + ZVU (left) and low-cost IMU + ZVU + adaptive-CHAIN (right)

To compare the overall accuracy epoch by epoch with a reliable ground reference, Trial 3 was conducted. Walking along the sideline of a square pitch for 10 rounds, the trial lasted for about 40 minutes for a total distance of about 3 km. The pedestrian started and stopped at the same position. The trial was performed outdoors so that a ground reference from GPS-Real Time Kinematic (RTK) system can be used, where the Leica GPS 1200 RTK system used gives a typical position accuracy of approximately 2 cm. Fig. 7 shows the position error between CHAIN (top) and adaptive-CHAIN (bottom). The oscillations that occurred are a result of a full round of walking (there are 10 peaks which are equivalent to 10 rounds of walking). Using RPE indicator, for CHAIN, the RPE was computed to be 3.52 m, while the adaptive-CHAIN improves remarkably to only 0.70 m in RPE, which is only about 0.02 % of the total distance travelled. This results in an ~80% improvement in the RPE. This is considered very significant considering the low-cost IMU was not aided by any other external sensors for a very long period of time. The maximum horizontal position error for both is also shown to be less than 5 m position error. The horizontal position RMSE for CHAIN is calculated to be 1.99 m. Albeit similar, the proposed adaptive-CHAIN shows slight improvement to 1.82 m. Note that the vertical position error is not considered in this work, where similar result can be found for example in [22].

5. Discussion

An approach to using the Multiple Polygon Areas (MPA) with adaptive weighted noise covariance was explored and three trials were undertaken to demonstrate its advantage. It resulted in a significant improvement in horizontal position accuracy for the low-cost foot mounted IMU. Note that the figure represents the RPE (difference between start and end position), and not the accuracy of the system throughout the trial. However, it did follow the correct trajectory throughout the whole trials.

The MPA was created to gather heading data for a huge navigation area with different building orientations. This can be very useful for a pedestrian who wants to cross between these buildings. While the basic CHAIN algorithm requires that each building heading is to be derived, this work introduced a way to reduce the complexity of having multiple heading data for each building. This is done by working out the same heading area using a polygon that consists of several buildings with the same heading. This does not mean that buildings need to be exactly identical to each other, but more towards having the same orientation to have the same heading value.

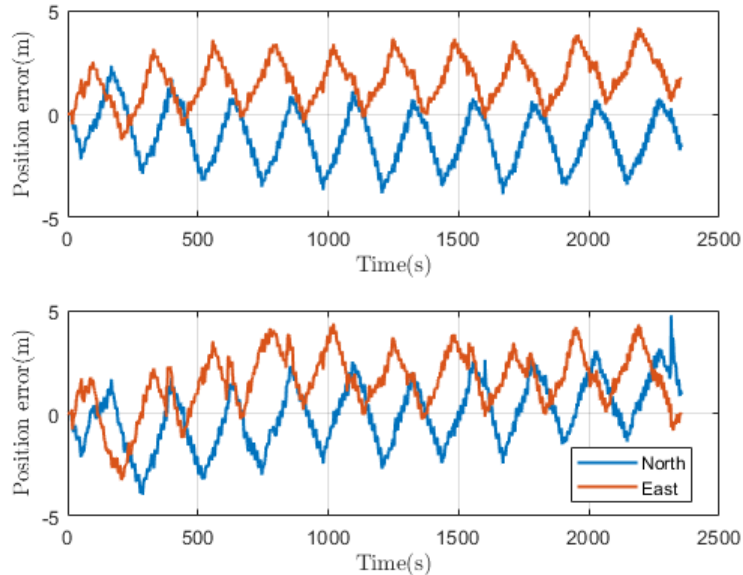


Fig. 7 - The horizontal position error for CHAIN (top) and the proposed adaptive-CHAIN (bottom)

The algorithm is further strengthened by incorporating an adaptive measurement noise covariance. The algorithm therefore diminishes overconfidence in the heading observation. For example, if the values selected are too small, the actual errors in the Kalman filter estimates will be much larger than the state uncertainties obtained from P. Conversely, if the values selected are too large, the reported uncertainties will be too large.

Although the motivation was to have a self-contained autonomous low-cost foot-mounted IMU, it is important to highlight the advantage of having extra measurements to the overall solution accuracy. Assuming a straight walk most of the time, there will be a time when this assumption may not be valid; for example during long cornering (although the algorithm is shown to work fairly well during trials). The uncompensated heading error will build due to increased uncertainty in the KF and cause a position drift error during this period. Thus, an occasional absolute position update might be useful for the system to correct its position drift (note that using the KF provides the ability to combine all available measurements). This could be done if, for example, one could figure out a reliable position from the degraded GNSS signal, or simply by walking into an open space in between buildings, where the GNSS can provide a reliable and accurate position solution. Another possible example would be to have a little more information from the map (again not a detailed map) such as having true positions (coordinates) of a building entrances and exits. This could correct some position drifts if a user can be identified to have indeed passed these entrances or exits.

Further work should highlight a point where more precise boundary detection should be made for polygon area creation when buildings of different headings are not well separated. The results presented herein are only the output of coarse creation of the polygon area. If a more accurate position solution is sought in a closely separated environment, better detection and polygon creation should be applied to update the correct heading. For example, let's consider an extreme scenario as depicted in Fig. 8. Suppose a low-cost foot-mounted IMU has a system accuracy of 5 m, and two buildings with different headings are separated with less than 5 m from each other. Due to the inaccuracy in the low-cost foot-mounted IMU, the position has drifted into the green building (a black arrow). This creates problem because when adaptive-CHAIN is applied, wrong position solution will be computed (red arrow) when the pedestrian walks in the green building.

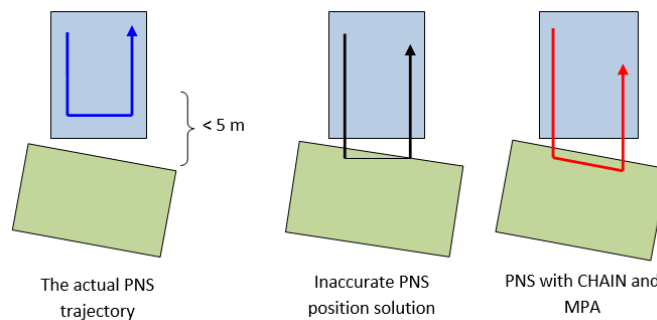


Fig. 8 - Extreme scenario when MPA causes problem to the overall Pedestrian Navigation System (PNS) solution

6. Closing Remarks

This paper extended authors' previous approach of using building heading information in a Kalman filter to restrict heading drift errors for a low cost autonomous foot-mounted IMU system. This is to highlight a case where users might need to cross between buildings that have different orientation. The fusing of building heading in Kalman filter environment was briefly explained. Then, using Multiple Polygon Areas with adaptive weighted measurement noise covariance, three trials were performed to demonstrate its effectiveness in increasing position accuracy. It resulted in a significant improvement in position accuracy for low cost indoor pedestrian navigation. It was shown that the estimated accuracy in position is consistently less than 5 m, for a 30 to 40-minutes' walk. Against the original CHAIN, the newly proposed adaptive-CHAIN improves remarkably in RPE, from 3.52 m to 0.7 m, which is only about 0.02 % from the distance travelled.

Acknowledgement

Financial support via the Ministry of Higher Education of Malaysia and Universiti Sains Islam Malaysia is graciously acknowledged.

References

- [1] P. Xie and M. G. Petovello, (2015). Measuring GNSS multipath distributions in urban canyon environments, *IEEE Trans. Instrum. Meas.*, doi: 10.1109/TIM.2014.2342452
- [2] M. Ren.K. Pan.Y. Liu.H. Guo.X. Zhang.and P. Wang, (2016). A novel pedestrian navigation algorithm for a foot-mounted inertial-sensor-based system, *Sensors (Switzerland)*, doi: 10.3390/s16010139
- [3] Z. Deng.P. Wang.T. Liu.Y. Cao.and B. Wang, (2020). Foot-Mounted Pedestrian Navigation Algorithm Based on BOR/MINS Integrated Framework, *IEEE Trans. Ind. Electron.*, doi: 10.1109/TIE.2019.2921275
- [4] K. Wen.K. Yu.Y. Li.S. Zhang.and W. Zhang, (2020). A New Quaternion Kalman Filter Based Foot-Mounted IMU and UWB Tightly-Coupled Method for Indoor Pedestrian Navigation, *IEEE Trans. Veh. Technol.*, doi: 10.1109/TVT.2020.2974667
- [5] N. Yu.Y. Li.X. Ma.Y. Wu.and R. Feng, (2019). Comparison of Pedestrian Tracking Methods Based on Foot- and Waist-Mounted Inertial Sensors and Handheld Smartphones, *IEEE Sens. J.*, doi: 10.1109/JSEN.2019.2919721
- [6] S. Liu *et al.*, (2018). Pedestrian indoor navigation using foot-mounted IMU with multi-sensor data fusion, *Int. J. Model. Identif. Control*, doi: 10.1504/IJMIC.2018.095833
- [7] X. Tong *et al.*, (2020). A double-step unscented kalman filter and HMM-Based zero-velocity update for pedestrian dead reckoning using MEMS sensors, *IEEE Trans. Ind. Electron.*, doi: 10.1109/TIE.2019.2897550
- [8] Y. Wang and A. M. Shkel, (2019). Adaptive Threshold for Zero-Velocity Detector in ZUPT-Aided Pedestrian Inertial Navigation, *IEEE Sensors Lett.*, doi: 10.1109/LSENS.2019.2946129
- [9] M. Ma.Q. Song.Y. Gu.Y. Li.and Z. Zhou, (2018). An adaptive zero velocity detection algorithm based on multi-sensor fusion for a pedestrian navigation system, *Sensors (Switzerland)*, doi: 10.3390/s18103261
- [10] R. Zhang.H. Yang.F. Höflinger.and L. M. Reindl, (2017). Adaptive Zero Velocity Update Based on Velocity Classification for Pedestrian Tracking, *IEEE Sens. J.*, doi: 10.1109/JSEN.2017.2665678
- [11] M. Luy.E. Cam.I. Uzun.and F. Ulamis, (2017). Effects of Zero Velocity Update on Total Displacement for Indoor Inertial Positioning Systems, *Int. J. Intell. Syst. Appl. Eng.*, doi: 10.18201/ijisae.2017528729
- [12] Y. Guo *et al.*, (2020). Improved Heuristic Drift Elimination Algorithm Optimisation Based on a Smartphone Gyroscope, *J. Navig.*, doi: 10.1017/S0373463319000821
- [13] D. Chai.G. Chen.and S. Wang, (2019). A novel method of adaptive Kalman filter for heading estimation based on an autoregressive model, *Appl. Sci.*, doi: 10.3390/app9183727
- [14] M. N. Muhammad.Z. Salcic.and K. I. K. Wang, (2018). Indoor Pedestrian Tracking Using Consumer-Grade Inertial Sensors with PZTD Heading Correction, *IEEE Sens. J.*, doi: 10.1109/JSEN.2018.2833118
- [15] Z. A. Deng.G. Wang.Y. Hu.and D. Wu, (2015). Heading estimation for indoor pedestrian navigation using a smartphone in the pocket, *Sensors (Switzerland)*, doi: 10.3390/s150921518
- [16] M. Ilyas.K. Cho.S. H. Baeg.and S. Park, (2016). Drift reduction in pedestrian navigation system by exploiting motion constraints and magnetic field, *Sensors (Switzerland)*, doi: 10.3390/s16091455
- [17] S. Cardarelli.P. Di Florio.A. Mengarelli.A. Tigrini.S. Fioretti.and F. Verdini, (2019). Magnetometer-Free Sensor Fusion Applied to Pedestrian Tracking: A Feasibility Study, 2019, doi: 10.1109/ISCE.2019.8901014
- [18] W. Qiuying.G. Zheng.Z. Minghui.C. Xufei.W. Hui.and J. Li, (2018). Research on Pedestrian Location Based on Dual MIMU/ Magnetometer/ Ultrasonic Module, 2018, doi: 10.1109/PLANS.2018.8373428
- [19] X. Cui.Y. Li.Q. Wang.M. Zhang.and J. Li, (2018). Three-axis magnetometer calibration based on optimal ellipsoidal fitting under constraint condition for pedestrian positioning system using foot-mounted inertial sensor/magnetometer, 2018, doi: 10.1109/PLANS.2018.8373378
- [20] Z. Li.C. Song.J. Cai.R. Hua.and P. Yu, (2018). An improved pedestrian navigation system using IMU and magnetometer, 2018, doi: 10.1109/ICCSEC.2017.8446992

- [21] K. Abdulrahim *et al.*, (2014). On magnetometer heading updates for inertial pedestrian navigation system, *Gyroscope Navig.*, vol. 5, no. 3, doi: 10.1134/S207510871403002X
- [22] K. Abdulrahim.C. Hide.T. Moore.and C. Hill, (2012). Using constraints for shoe mounted indoor pedestrian navigation, *J. Navig.*, vol. 65, no. 1, doi: 10.1017/S0373463311000518
- [23] J. Pinchin.C. Hide.K. Abdulrahim.T. Moore.and C. Hill, (2011). Integration of heading-aided MEMS IMU with GPS for pedestrian navigation, 24th Int. Tech. Meet. Satell. Div. Inst. Navig. 2011, ION GNSS 2011, vol. 2, pp. 1346–1356
- [24] K. Abdulrahim.C. Hide.T. Moore.and C. Hill, (2011). Aiding low cost inertial navigation with building heading for pedestrian navigation, *J. Navig.*, vol. 64, no. 2, doi: 10.1017/S0373463310000573
- [25] C. S. Ling.M. H. Ahmad.and D. R. Ossen, (2007). The effect of geometric shape and building orientation on minimising solar insolation on high-rise buildings in hot humid climate, *J. Constr. Dev. Ctries*
- [26] M. Wang.W. Wu.X. He.and X. Pan, (2019). State Transformation Extended Kalman Filter for SINS based Integrated Navigation System, in 2019 DGON Inertial Sensors and Systems (ISS), 2019, pp. 1–14
- [27] W. I. Liu.Z. Li.and Z. Zhang, (2019). Error modelling and optimal estimation of laser scanning aided inertial navigation system in GNSS-denied environments, *J. Navig.*, vol. 72, no. 3, pp. 741–758
- [28] A. R. Jiménez.F. Seco.F. Zampella.J. C. Prieto.and J. Guevara, (2012). Improved heuristic drift elimination with magnetically-aided dominant directions (MiHDE) for pedestrian navigation in complex buildings, *J. Locat. based Serv.*, vol. 6, no. 3, pp. 186–210
- [29] D. Titterton.J. L. Weston.and J. Weston, (2004)Strapdown inertial navigation technology, vol. 17. IET, 2004.
- [30] R. H. Rogne.T. H. Bryne.T. I. Fossen.and T. A. Johansen, (2020). On the Usage of Low-Cost MEMS Sensors, Strapdown Inertial Navigation, and Nonlinear Estimation Techniques in Dynamic Positioning, *IEEE J. Ocean. Eng*
- [31] J. Farrell, (2008)Aided navigation: GPS with high rate sensors. McGraw-Hill, Inc., 2008
- [32] J. Li.P. Dang.Y. Li.and B. Gu, (2018). A general Euler angle error model of strapdown inertial navigation systems, *Appl. Sci.*, vol. 8, no. 1, p. 74
- [33] E.-H. Shin, (2005). Estimation techniques for low-cost inertial navigation, 2005
- [34] B. M. Scherzinger and D. B. Reid, (1994). Modified strapdown inertial navigator error models, *Rec. - IEEE PLANS, Position Locat. Navig. Symp.*, pp. 426–430
- [35] C. Chen.W. Chai.A. K. Nasir.and H. Roth, (2012). Low cost IMU based indoor mobile robot navigation with the assist of odometry and Wi-Fi using dynamic constraints, in Proceedings of the 2012 IEEE/ION Position, Location and Navigation Symposium, 2012, pp. 1274–1279
- [36] T. Moore and D. Stouch, (2016). A generalized extended kalman filter implementation for the robot operating system, in *Intelligent autonomous systems 13*, Springer, 2016, pp. 335–348
- [37] R. Song.Z. Zhang.and H. Liu, (2017). Edge connection based Canny edge detection algorithm, *Pattern Recognit. Image Anal.*, vol. 27, no. 4, pp. 740–747
- [38] N. S. Aminuddin, (2020). A new approach to highway lane detection by using Hough transform technique, *J. Inf. Commun. Technol.*, vol. 16, no. 2, pp. 244–260
- [39] S. Yang.J.-H. Yong.J. Sun.H. Gu.and J.-C. Paul, (2010). A point-in-polygon method based on a quasi-closest point, *Comput. Geosci.*, vol. 36, no. 2, pp. 205–213
- [40] E. Lozowski et al., (2016). Comparison of IMU Measurements of Curling Stone Dynamics with a Numerical Model, 2016, doi: 10.1016/j.proeng.2016.06.246